



HAL
open science

Contrasting the evolution of radiation fog over a heterogeneous region in southwest France during the SOFOG3D campaign

J. Thornton, J D Price, Frédéric Burnet, C. Lac

► **To cite this version:**

J. Thornton, J D Price, Frédéric Burnet, C. Lac. Contrasting the evolution of radiation fog over a heterogeneous region in southwest France during the SOFOG3D campaign. Quarterly Journal of the Royal Meteorological Society, In press, 10.1002/qj.4558 . hal-04222658

HAL Id: hal-04222658

<https://hal.science/hal-04222658v1>




Submitted on 29 Sep 2023

HAL is a multi-disciplinary open access archive for the deposit and dissemination of scientific research documents, whether they are published or not. The documents may come from teaching and research institutions in France or abroad, or from public or private research centers.

L'archive ouverte pluridisciplinaire **HAL**, est destinée au dépôt et à la diffusion de documents scientifiques de niveau recherche, publiés ou non, émanant des établissements d'enseignement et de recherche français ou étrangers, des laboratoires publics ou privés.

RESEARCH ARTICLE

Contrasting the evolution of radiation fog over a heterogeneous region in southwest France during the SOFOG3D campaign

J. Thornton¹  | J. D. Price¹ | F. Burnet²  | C. Lac² ¹UK Met Office Research Unit,
Cardington Airfield, Shortstown, UK²CNRM, Université de Toulouse,
Toulouse, France**Correspondence**J. Thornton, UK Met Office Research
Unit, Cardington Airfield, Shortstown,
Bedfordshire, MK42 0SY, UK.
Email: jenna.thornton@metoffice.gov.uk**Abstract**

Observations made during the recent South-west FOGs 3D experiment (SOFOG3D) have been used to investigate the formation and evolution of radiation fog over heterogeneous forest plantations. The focus was on comparing measurements made at a relatively open site on arable land with those made in an approximately 700-m diameter field surrounded by tree plantations, with both sites hosting an instrumented 50-m mast. These data showed that at the more sheltered site radiation fog tended to form earlier than at the more open site. This coincided with more rapid decreases and lower minima in both near-surface temperatures and vertical turbulence from the late afternoon. It is proposed here that the surrounding forest creates a sheltering effect, which can cause a reduction in vertical turbulence and therefore the mixing of cool near-surface air with warmer air aloft. The near-surface region is therefore able to cool rapidly, enabling fog to form more readily. Data from additional sites with varying surroundings supported the findings that the more sheltered sites tended to exhibit lower near-surface nocturnal temperatures. However, the onset of fog formation observed at these additional sites suggested that there could be a limit to how sheltered a site may be before fog formation is inhibited rather than enabled by the surroundings.

KEYWORDS

fog, heterogeneous land use, radiation fog, sheltering, SOFOG3D, stable boundary layer

1 | INTRODUCTION

The effects of fog on human life and economic efficiency can be severe, and therefore the ability to forecast these events correctly is of great importance. Gulpepe *et al.* (2019) stated that fog is the second-most prevalent cause of aviation accidents due to weather, and Kulkarni

et al. (2019) estimated that between 2011 and 2016 in Delhi alone the economic loss to airlines due to fog was 3.9 million dollars. Fog can also have a severe impact on ground transportation; between 2002 and 2007, there were 299 fatal crashes in Florida due to fog (Ahmed *et al.*, 2014). In India in 2019 alone, 10,000 people were killed in fog-related road accidents (Kapoor, 2019).

This is an open access article under the terms of the [Creative Commons Attribution-NonCommercial](https://creativecommons.org/licenses/by-nc/4.0/) License, which permits use, distribution and reproduction in any medium, provided the original work is properly cited and is not used for commercial purposes.

© 2023 Crown copyright and Meteo-France. *Quarterly Journal of the Royal Meteorological Society* published by John Wiley & Sons Ltd on behalf of Royal Meteorological Society. This article is published with the permission of the Controller of HMSO and the King's Printer for Scotland.

Gultepe *et al.* (2007) states that, despite the economic losses for the transport industry due to fog being comparable with those caused by tornadoes, storms, and hurricanes, models still struggle to predict fog accurately due to a general lack of understanding of fog processes. In forecasts of photovoltaic power over Germany, Köhler *et al.* (2017) found that almost a third of errors were due to the modelling of fog and low stratus. Significant errors in modelling fog are expected to arise due to the difficulty in initiating the correct near-surface atmospheric variables (Tudor, 2010; Pu *et al.*, 2016; Chachere and Pu, 2019), followed by the complexities of modelling the boundary layer, radiation, and microphysics correctly to create the balance required for radiation fog formation (Van der Velde *et al.*, 2010; Steeneveld *et al.*, 2015). Steeneveld *et al.* (2010) found that with the fifth generation Pennsylvania State University-National Center for Atmospheric Research mesoscale model the boundary layer was poorly modelled, which resulted in surface temperatures and wind speeds that were too high. As part of the Local and Non-local Fog EXperiment (LANFEX) campaign, Smith *et al.* (2021) also found that the Met Office Unified Model (MetUM) output surface temperatures that were too high in the valleys in Shropshire, UK, whereas the surrounding hills were too cold. This resulted in too much fog being formed on the hills and not enough in the valleys. This temperature bias was present even when using a high horizontal resolution (100 m). Rotach and Zardi (2007) also found that, even when using a high horizontal resolution of less than 1 km, the Advanced Regional Prediction (ARPs) model output a turbulent boundary layer that was too shallow in the presence of complex terrain. These issues can occur even over relatively less complex terrain. At a site in Bedfordshire, UK, which sits in a large shallow valley of approximately 10 km diameter and is surrounded by arable fields, a radiation fog event was used in an intercomparison between Large-Eddy Simulation (LES) and single column models (Boutle *et al.*, 2022). This work revealed large differences between the model outputs in forecasting fog, where changes to the microphysics (i.e., cloud droplet number concentration) enhanced these discrepancies. At the same site, Smith *et al.* (2021) found that the MetUM model struggled to form the stable shallow radiation fog that had been observed, partly due to warm temperature biases in the model. In contrast, Van der Velde *et al.* (2010) found that the HIRLAM model was able to simulate the formation of fog, but was unable to develop a deep enough fog, which subsequently dissipated too early. A single-column version of HIRLAM run at various vertical resolutions showed that the lower resolution led to an underestimation of liquid water content, thus highlighting the requirement for high vertical resolution to forecast fog formation accurately.

In order to improve the effectiveness of models in predicting fog correctly, further observation-based work must be carried out to understand the mechanisms involved at each stage from formation to dissipation of fog. In this work we focus on the formation, evolution, and dissipation of radiation fog specifically. Radiation fog forms due to radiative cooling near to the surface (Roach *et al.*, 1976) in the presence of low winds (Roach *et al.*, 1976; Cuxart and Jiménez, 2012) and low turbulence and heat fluxes (Roach, 1995; Gultepe *et al.*, 2016; Price, 2019). Price (2019) observed that vertical velocity variance values lower than approximately $0.002\text{--}0.005\text{ m}^2 \cdot \text{s}^{-2}$ were required for radiation fog to form. If these conditions are met, then shallow stable radiation fog can form. This fog initially forms within a temperature inversion; however, as the fog develops vertically and becomes optically more dense, radiative cooling has a greater influence at the fog top than at the surface. This causes the temperature inversion to erode and the temperature profile to become saturated adiabatic. Price (2011) found that, in 47% of radiation fog cases observed at a site in Bedfordshire, UK, on average it took 3.4 hr for fog to become deep adiabatic from initial formation. The timing of this transition to deep adiabatic can be influenced by the humidity, wind speed, turbulence (Smith *et al.*, 2018), and microphysics. During the LANSFEX campaign, Price, 2019 found that, in some cases, if the turbulence increased then the shallow stable fog would dissipate. When the fog has become deeper, however, an increase in turbulence is observed and tolerated (Price, 2011; Bergot, 2013; Price, 2019). Once these deeper fogs have formed, they can persist throughout the day (Price, 2011) and sometimes even over multiple days (Cuxart and Jiménez, 2012). The eventual dissipation of this fog can be driven by heating of the surface due to solar insolation (contribution from shortwave and longwave radiation: (Wærsted *et al.*, 2019) or longwave heating from the surface (Price, 2011; Cuxart and Jiménez, 2012), higher cloud above, or changes in large-scale conditions, that is, wind speed. Wærsted *et al.* (2019) used observations made at Site Instrumental de Recherche en Télédétection Atmosphérique (SIRTA) to set up fog conditions from sunrise in the Dutch Atmospheric Large-Eddy Simulation model (DALES) and, after simulations had been executed, found that the most dominant source of dissipation was from surface turbulent heat fluxes, that is, sensible heat flux. The dissipation of fog can occur rapidly a few hours after sunrise and can result in the entire fog layer dissipating (Haeffelin *et al.*, 2010), if large-scale condition changes have not occurred previously.

Recent field campaigns have been executed, such as ParisFOG (Haeffelin *et al.*, 2010), LANSFEX (Price, 2011), and Fog Remote sensing and Modelling (FRAM: (Gultepe *et al.*, 2009), for which the life cycle of fog has been

studied. During the former two, the effect of heterogeneity on fog was investigated. As part of ParisFOG, measurements were made over three different zones at the SIRTa observatory; the zones included (1) an area of small-scale surface heterogeneities, (2) an area of buildings, and (3) a more open area. During LANFEX, multiple measurement stations were set up in valleys and at hill tops and supplemented by data from a relatively flat area; the effect of orographic heterogeneity on the fog life cycle was studied. The work presented here took advantage of measurements made during the SOuth-west FOGs 3D experiment (SOFOG3D) field campaign. These were made over a relatively flat and more extensive area of land in southwest France, characterised by heterogeneity in the form of a mixture of open sites with grass or winter crops and more forested sites. Roach (1995) stated that both surface type and larger-scale roughness, that is, woods and buildings, can have an influence over radiation fog formation. Cold pooling in valleys affects both the timing and the density of radiation fog (Scherrer and Appenzeller, 2014; Price, 2019). Pauli *et al.* (2022) used satellite data at a regional scale to observe that nocturnal fog and low stratus were more common over the Landes Forest than in the surrounding areas, likely due to lower temperatures and lower winds. Mazoyer *et al.* (2017) found that, at a local scale, forested areas can affect the occurrence of fog; through sensitivity studies of a 5-m horizontal resolution and 1-m vertical resolution simulation of a radiation fog event, they found that removal of both the tree barrier that was within 100 m of the measurement site and deposition onto the forest canopy resulted in fog formation that occurred 2 hr earlier than was observed. Additionally, at the field site set up as part of the ParisFOG campaign, Mazoyer *et al.* (2017) simulated that the fog formed first at the surface upstream and 500 m downstream of the forested area, and initially only formed at elevated levels over the forest clearing, in agreement with observations. Surface heterogeneity can have a large influence over the formation and evolution of radiation fog, but, so far, detailed observational studies into the effect of different land cover on fog development are rare and a clear description of the influence of proximity to the forest does not exist at a local scale.

The objective of this study is to provide a better understanding of the impact of forest proximity on the fog life cycle by comparing measurements of radiative fog cases at different sites which vary in their degree of sheltering by surrounding forests. We use data from the recent SOFOG3D field campaign, which are described in Section 2. Two radiation fog cases are presented in Section 3, for which data are compared from ground level up to 50 m at two different sites. Additional radiation fog cases at the two sites are then evaluated at the near-surface

only in Section 3.6. Finally, in Section 4 we introduce additional sites to explore further the effect of different degrees of sheltering on radiation fog formation.

2 | STUDY AREA AND DATA COLLECTED

The observations used here were made as part of the SOFOG3D campaign (Burnet *et al.*, 2020),¹ which had the overarching aim of understanding fog processes better at small scales. The aims of the project were set to be realised through an initial six-month long field campaign (now completed), followed by a longer period of data analysis. The field campaign took place from the autumn of 2019 to the spring of 2020 over southwest France and captured the fog variability on both horizontal and vertical scales.

The main study area covered a region approximately 50 × 50 km, which consisted of 17 meteorological stations, with 10 of these being hosted within a smaller domain of 10 × 10 km. The area consisted of an essentially level plain before rising to the east, and topographically it consisted of mostly forest plantations interspersed by large areas of arable land. The forest plantations consisted of relatively small blocks of conifer trees (up to approximately 20 ha) of varying ages and heights (from saplings up to approximately 20 m tall). Given the simple, flat orography in the immediate region, it was expected that the effects of the heterogeneous forest plantations on fog formation could be determined, and this formed one of the key aims of the SOFOG3D study experiment.

An extensive suite of instrumentation was deployed over the region. This consisted of two large supersites with 50-m masts, capable of measuring the energy balance and various microphysical properties of fog, and a range of smaller stations, some capable of eddy-covariance measurements. The two 50-m mast sites are referred to as Le Couye and Jachere, and were managed by the UK Met Office (UKMO) and Météo-France, respectively. These two sites were situated 6.7 km from each other, point to point, and lay at similar elevations of 68 m at Jachere and 70 m at Le Couye. One major difference between the sites was their surroundings; whereas the site at Le Couye was in a field (approximately 700 m across) that was surrounded by forested area with treetops at around 10–20 m high, the site at Jachere was on arable land that was open and unobstructed in most directions, with the exception of a small forested area to the north. Figure 1 shows the view towards the southwest at both sites.

¹SOFOG3D project website: https://www.umn-cnrm.fr/spip.php?article1086#outil_sommaire_5, last access 26 September 2022.

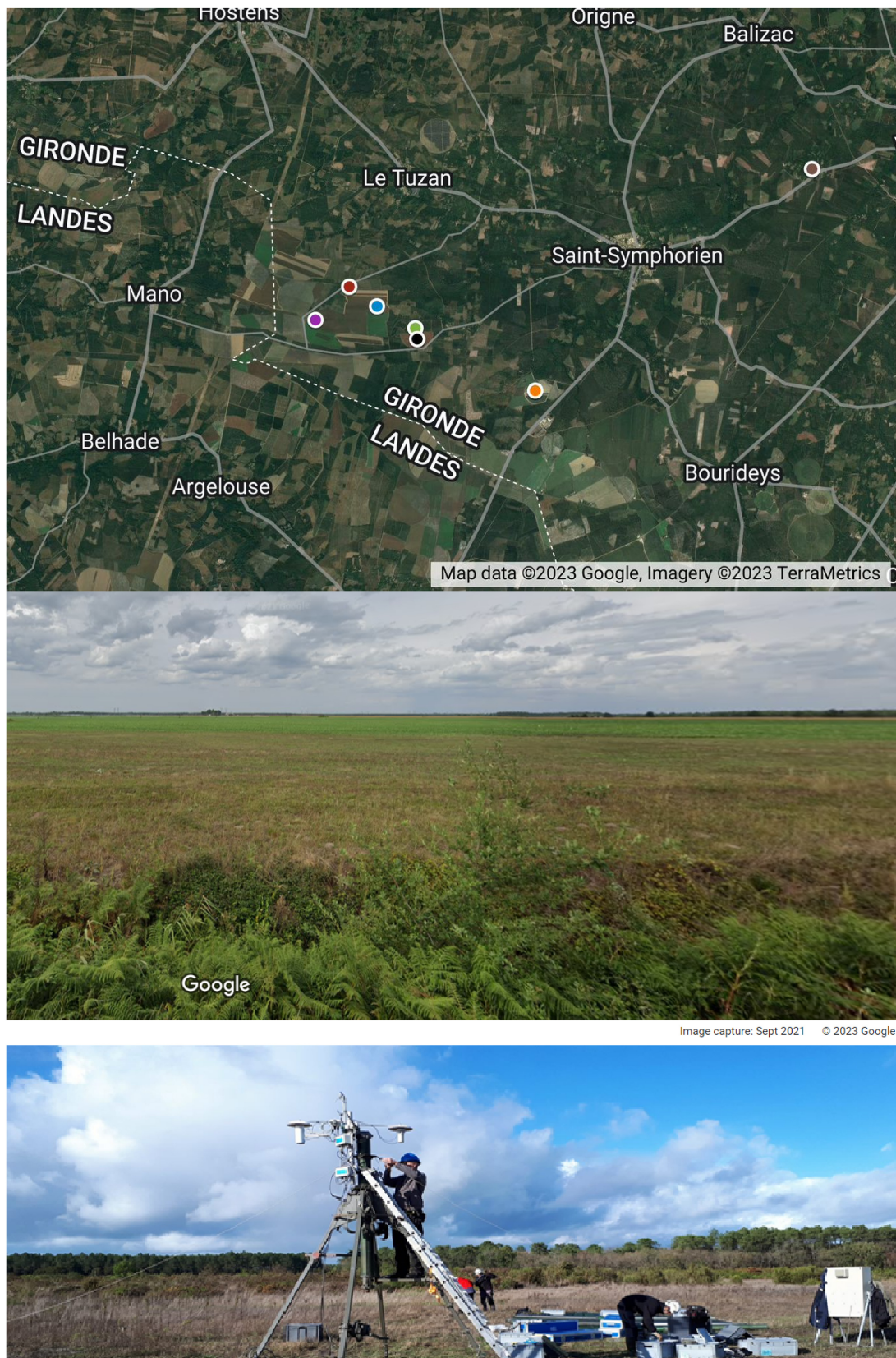


FIGURE 1 The top panel shows the locations of each of the SOFOG3D measurement sites for which data were used in the analysis presented here. The two 50-m mast sites, Le Couye and Jachere, are represented by the orange and purple markers, respectively. The additional sites are Charbonniere (red), Basta fog monitor station (blue), Champs-Tanon fog monitor station (black), Les Houzins (brown), and Foret-Tanon (green). The middle and bottom panels are photos looking southwest at Jachere and Le Couye, respectively.

These two sites are the main focus of the work presented here; however, additional sites were also used to supplement these. The five additional sites were chosen to represent a range of smaller and larger areas within or adjacent to the forested area. All of the sites used in this analysis were contained within an area of around 7×15 km (Figure 1).

At both Le Couye and Jachere, instrumentation WAS deployed from subsoil to approximately 50 m high. The core measurements used in this study were collected at the following heights.

- (i) 3D wind speed and direction: at 48, 23, 10, and 2 m at Le Couye and 50, 25, 10, and 3 m at Jachere.
- (ii) Air temperature: 48, 23, 10, and 1.2 m at Le Couye and 45, 25, 10, and 2 m at Jachere. Skin-temperature measurements were not available at Jachere.
- (iii) Visibility: 48, 23, and 2 m at Le Couye and 48, 25, and 3 m at Jachere.

Relative humidity (RH) values were also available at the heights described in (ii); however, due to calibration uncertainties at Le Couye we have chosen not to use these in this work. We have, however, used these values to convert the RH into specific humidity (Q), where the data were deemed to be of sufficient quality.

From these data, heat fluxes and turbulence intensity were also calculated. Additionally, we used radiative fluxes at 2 and 1 m at Le Couye and Jachere, respectively, and soil heat-flux measurements made at 2 cm below the surface at both sites. The measurements that were collected above 10 m at Jachere were only available up until early November 2019, after which data were only available at 10 m or below.

The additional sites were used for comparison of the near-surface conditions only; these consisted of the following.

- (i) Visibility: at 3 m at Charbonniere, Les Houzins, and Foret-Tanon; there were no visimeters at Basta or Champs-Tanon fog monitor stations (FMS).
- (ii) Air temperature: at 2 m at Charbonniere, Les Houzins, and Foret-Tanon, and 1.2 m at Basta FMS and Champs-Tanon FMS.
- (iii) Longwave radiation: at 1 m at Les Houzins and Foret-Tanon.

The additional sites did not host as extensive a suite of instrumentation as Le Couye and Jachere, that is, heat fluxes and turbulence intensity were not available. These sites have therefore been used to supplement the findings from Le Couye and Jachere, rather than being used to introduce the concepts discussed in the following sections.

The data from Jachere, Charbonniere, Les Houzins, and Foret-Tanon sites were collected, processed, and provided by Meteo-France; those from Le Couye, Basta FMS, and Champs-Tanon FMS were collected and processed by the UK Met Office. A list of instrumentation located at the UK Met Office and Meteo-France sites, along with their associated uncertainties and sampling and logging frequencies, is provided in the Appendix.

3 | COMPARISON BETWEEN OPEN AND SHELTERED SITES

3.1 | Case studies

Presented here are data from both of the 50-m mast sites, Le Couye and Jachere, for two cases of radiation fog formation and development during October 2019. The two fog events occurred on consecutive nights, one beginning on the evening of October 28 and ending on the morning of October 29, and the second beginning on the evening of October 29 and ending on the morning of October 30. Both fog events were observed at Le Couye and Jachere and developed into deep fog, which grew to at least 50 m in height, according to visibility measurements and infrared (IR) camera footage. The IR camera mounted at 48 m above the ground at Le Couye showed that the former case was that of in situ fog formation that was later affected by nonlocal cloud advecting over the site and resulting in the development of deep fog. The latter was a case of in situ development of a deep fog layer.

Analysis of MetUM surface pressure charts indicated that during October 28 and 29, 2019, a high-pressure system over the UK and the north of France and one towards the south of Spain kept neighbouring low-pressure systems out towards the west beyond the SOFOG3D area. This resulted in generally low winds, low temperatures, and dry conditions at the measurement sites during late afternoon on October 28 to late morning on October 30. A trough can be seen over the measurement area on October 28 at midday, but this appears to have passed by late afternoon. Very calm easterlies that were present on October 28 became even calmer northerlies on October 29, eventually changing back to easterlies by sunrise on October 30.

3.2 | Fog formation and dissipation

At Le Couye, fog started to form in situ in the late afternoon during both cases. Data from lidar and images from the IR camera showed that the initial fog that had formed was dissipated by cloud passing overhead (causing the surface region to warm). This happened for each even,

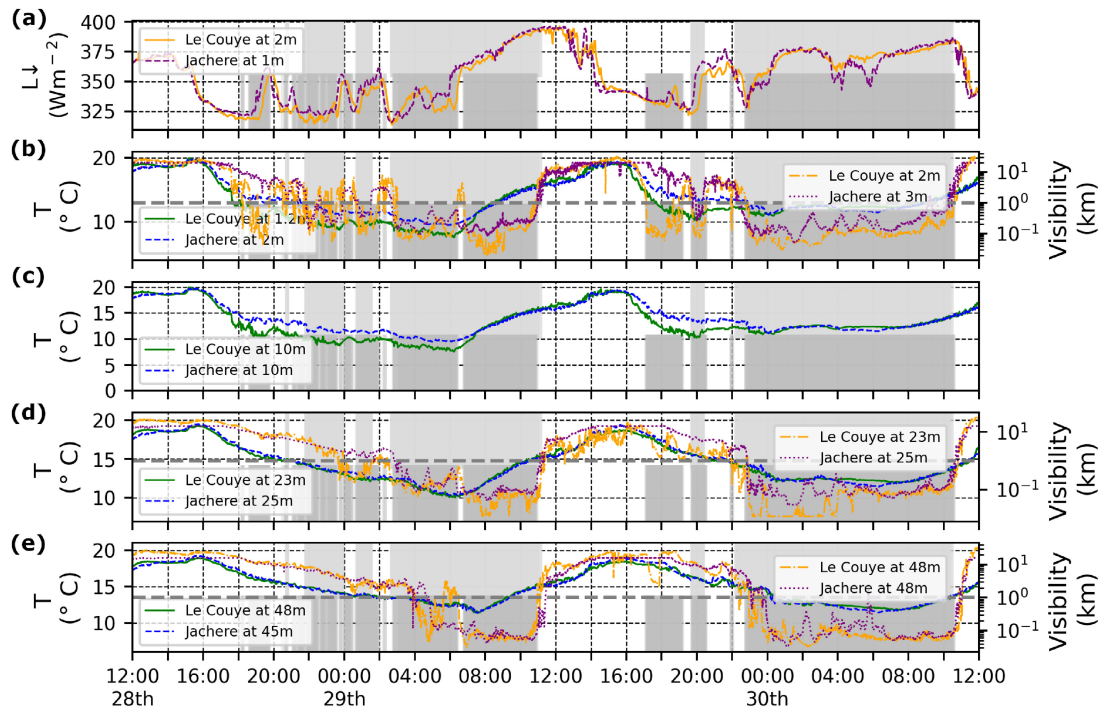


FIGURE 2 (a) Downwelling longwave radiation measured at 2 m at Le Couye and 1 m at Jachere; (b) visibility and temperature at the near-surface at Le Couye (orange and green, respectively) and Jachere (purple and blue, respectively), (c) temperature only at 10 m at both Le Couye and Jachere, and the visibility and temperature at (d) 23 m at Le Couye and 25 m at Jachere, and (e) 48 m at Le Couye and 48 m and 45 m at Jachere, respectively. The grey shading in the top and bottom halves of each plot represents the times at which fog was present between October 28 and October 30, 2019 at the level of the lowest visiometer at Jachere and Le Couye, respectively. The horizontal dashed lines in (b), (d), and (e) represent where visibility is equal to 1 km, the threshold for fog.

with initial fog formation occurring at 1800 and 1700 UTC and dissipation at 2000 and 1900 UTC on October 28 and 29, respectively. Once the cloud had completely passed over the site, the fog quickly reformed during both cases. On October 28, this occurred at around 2200 UTC, after which time the fog remained inhomogeneous until around 0600 UTC, when stratus fog appeared to lower and move over the existing fog. On October 29, the fog that had reformed after the cloud had passed at around 2000 UTC, dissipated quickly due to additional cloud moving over the site. The fog did, however, reform in situ for a second time after the overhead cloud had passed at 2200 UTC. After this point the fog became deep-adiabatic relatively quickly, by around 0200 UTC. For both cases, the time at which the fog reformed for the first time at Le Couye coincided with that at which fog first formed that evening at Jachere, at around 2200 UTC on October 28 and 2000 UTC on October 29. The similar trends in near-surface downwelling longwave radiation at both Le Couye and Jachere are suggestive of cloud passing over both sites within similar timeframes (Figure 2a).

The early in situ fog formation on both dates at Le Couye remained shallow, having only been observed by the visiometer at 2 m and not at 23 or 48 m, as shown in Figure 2b–e. On October 29, however, reductions in

visibility down to between 3 and 1 km were observed at heights of 23 and 48 m, therefore suggesting that fog might have developed vertically very rapidly after it had first formed if the cloud had not passed over the site, causing it to dissipate. Note that, on both dates, fog formed first at Le Couye. Further analysis (below) indicates that this was a typical result. We discuss a possible cause for this in the following sections.

For both radiation fog cases, the lifting of fog to stratus occurred at approximately the same time at both sites, between 1000 and 1100 UTC. The sunrise occurred at around 0630 UTC, as can be seen by the gradually increasing shortwave downwelling ($S \downarrow$) radiation in Figure 3a. The σ_w^2 began to increase significantly after temperature convergence occurred, as expected when a fog transitions from a stable to a weakly unstable deep-adiabatic fog (Price, 2019), but the temperatures did not begin to increase consistently until after sunrise. The data therefore suggest that incoming shortwave radiation after dawn was the cause of the temperature increase and eventual fog lifting, but increased turbulence and mixing with dry air above the fog may also have aided this. In agreement with previous studies (Mazoyer *et al.*, 2017), there is no contrast between both sites at the time of dissipation.

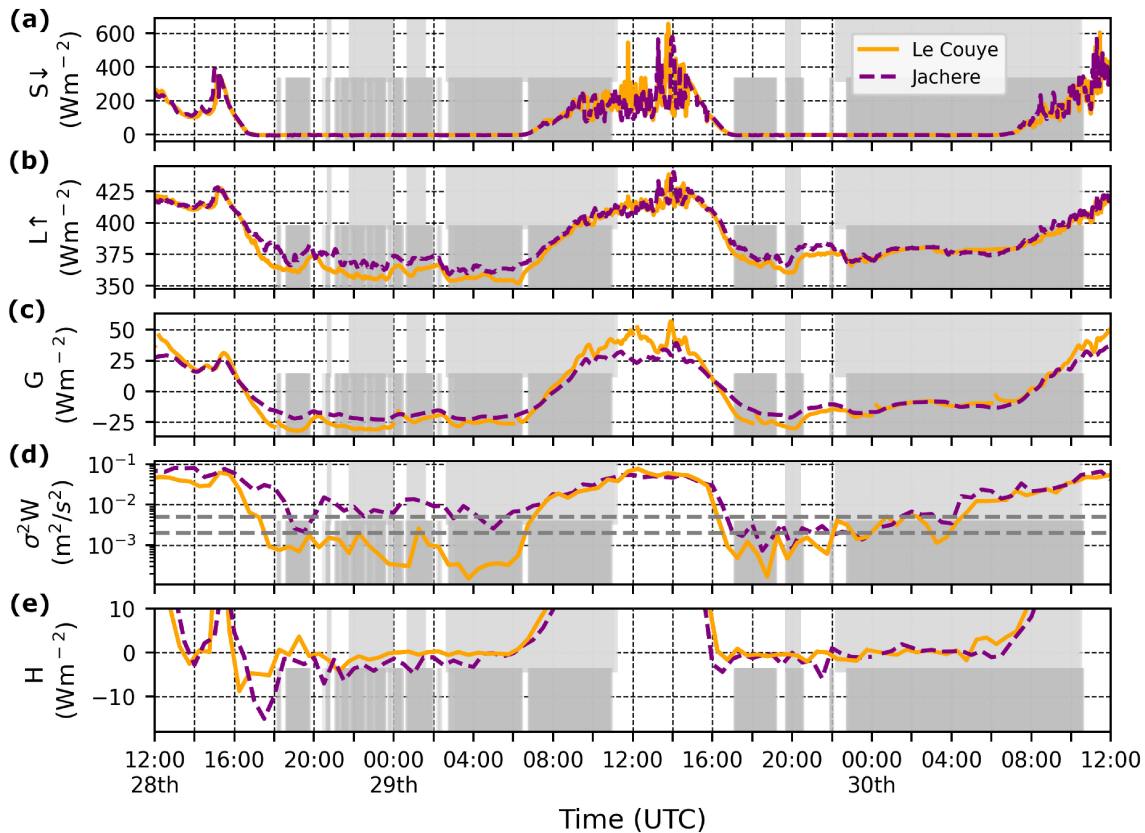


FIGURE 3 (a) Downwelling shortwave radiation, (b) upwelling longwave radiation, (c) soil heat flux, (d) vertical velocity variance, and (e) sensible heat flux at Le Couye and Jachere during both October radiation fog cases; the solid orange and dashed purple lines show the observations at Le Couye and Jachere, respectively. The dashed horizontal lines in (d) represent the two threshold values of 0.002 and $0.005 \text{ m}^2 \cdot \text{s}^{-2}$ (Price, 2019).

3.3 | Temperature

By 1600 UTC on both October 28 and 29, and at both sites, the air temperature at all heights above ground started to decline, as shown in Figure 2b–e. The rate at which the temperature dropped differed between sites near the surface, but generally agreed at higher measurement heights above 10 m. At Le Couye, on October 28, the temperature at 1.2 m dropped rapidly by around 8°C by the time that fog started to form at low levels; the 2-m temperature at Jachere remained 2°C higher at this point. Similarly, on October 29 the near-surface temperature at Jachere was 2°C higher than that at Le Couye by the time fog started to form at the latter site. For this case, the drop in temperature at Le Couye was around 5°C by the time fog formed (around an hour earlier than on October 28). After this initial more rapid decline in near-surface temperature at Le Couye, the temperature at this height continued to fall more rapidly than at Jachere and ultimately reached lower values. These lower temperatures at Le Couye relative to Jachere were then maintained until around the time that the fog became deep-adiabatic on October 28, and around an hour before this occurred on October 29.

The time at which the fog became deep-adiabatic is illustrated in Figure 4, and occurred when temperatures at multiple heights can be seen to converge. For the case on October 29, convergence happens during the night at around 0200 UTC, when temperatures increased significantly at lower levels. This was radiatively driven, due to fog thickening causing more cooling at the fog top than at the surface, and therefore eroding the temperature inversion. The convergence on October 28, however, did not occur until around 0730 UTC on October 29. The reason for the convergence is not clear; it could have been a consequence of stratus fog lowering over the existing radiation fog and merging with it, as seen in the ceilometer backscatter and IR camera footage, or alternatively due to solar insolation.

In contrast to the differences in temperatures measured at the near-surface between the two sites, those at 10 m and above at Le Couye were much more similar to those at the corresponding heights at Jachere. However, this is a more robust statement when addressing the temperatures at 23 m and above; at 10 m there were exceptions. Generally the 10-m temperatures at both sites were similar, but there were times during both cases where the

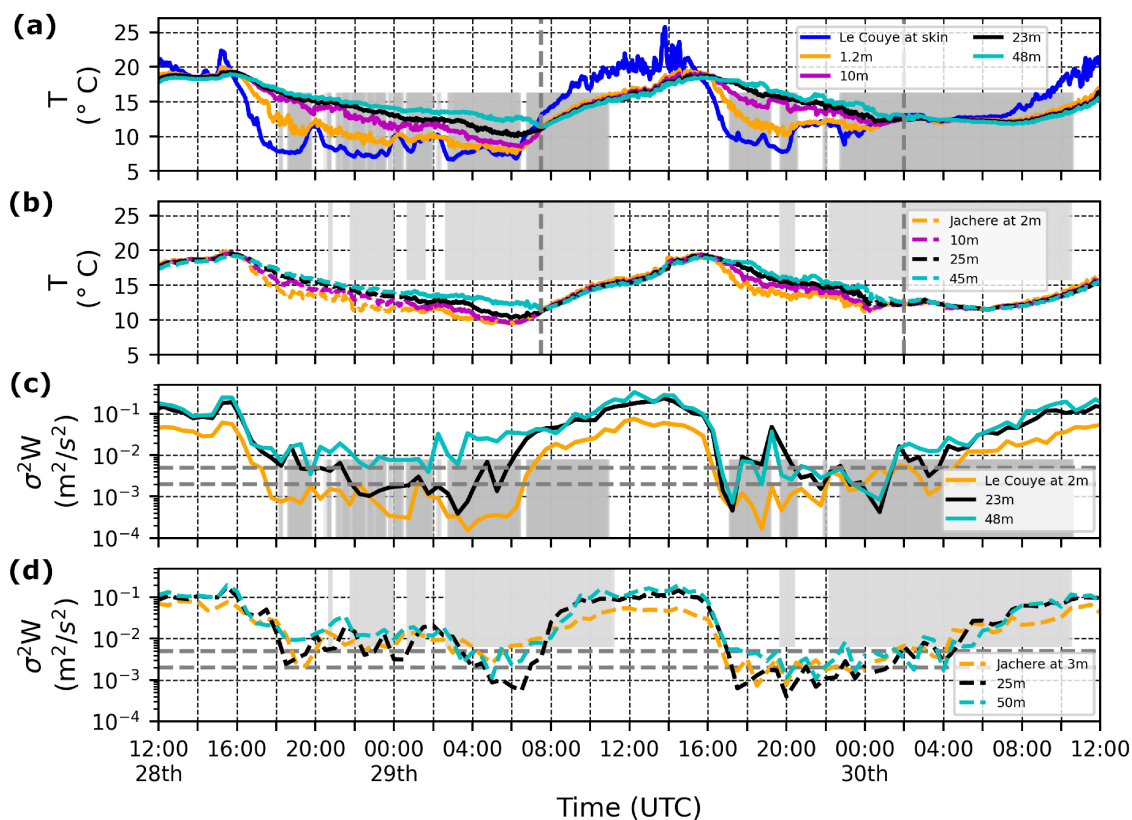


FIGURE 4 (a) Skin temperature (blue) and air temperature measured at 1.2 m (orange), 10 m (magenta), 23 m (black), and 48 m (cyan) at Le Couye, and (b) air temperature measured at 2 m (orange), 10 m (magenta), 25 m (black), and 45 m (cyan) at Jachere. The vertical dashed lines represents approximately when temperature convergence occurred. Also shown is the vertical velocity variance at (c) 2 m (orange), 23 m (black), and 48 m (cyan) at Le Couye, and (d) 3 m (orange), 25 m (black), and 50 m (cyan) at Jachere during the two cases of radiation fog in October 2019. The dashed horizontal lines represent the threshold for fog formation as described by Price (2019).

temperatures were seen to cool more quickly at Le Couye. It appears that 10 m is a transition height between differences of temperature.

Where the 10-m temperature at Le Couye did drop more rapidly on October 29, the visibility at 23 m at Le Couye did reduce towards 1 km during the early fog-formation event, which may have been a consequence of more rapid cooling above the near-surface height, that is, at 10 m. This relative reduction in temperature at Le Couye, however, is shorter lived than that at the near-surface. Given that early low-level fog formation was not seen at Jachere and that the near-surface temperatures did not drop as low or as rapidly, it is possible that this more efficient cooling near the surface at Le Couye is enabling fog to form here. We discuss in the following section why this rapid cooling at Le Couye could have occurred.

3.4 | Turbulence and heat fluxes

The downwelling (\downarrow) longwave (L) radiation at the near-surface at both Le Couye and Jachere is shown in

Figure 2a. The plot illustrates that there was not much difference between the downwelling longwave radiation measured at both sites from the late afternoon until fog formed and, where there were minor differences, these may be expected due to slight random variations in cloud cover. The maximum difference in downwelling longwave radiation between the sites was approximately $20 \text{ W}\cdot\text{m}^{-2}$ occurring at 1800 UTC on October 28. The soil heat flux shown in Figure 3c, where negative represents heat moving towards the surface, was driven by the temperature gradient and was therefore more negative at Le Couye, as a consequence of the colder screen-level temperatures. The greater amount of upward soil heat flux at Le Couye, present by 1700 UTC and lasting multiple hours over both cases, was a response to greater cooling at the surface. The upwelling (\uparrow) longwave (L) radiation at the near-surface at both sites is shown in Figure 3b. There are small differences between the upwelling longwave measurements at both sites, which are expected to be caused by the difference in near-surface temperatures at the two sites: there was more upwelling longwave radiation at Jachere when the screen-level temperatures were warmer than those

at Le Couye. Therefore, given that the greater upward soil heat flux at Le Couye was a consequence of colder screen-level temperatures and the upwelling longwave radiation was less than at Jachere (radiative fluxes were measured at 2 and 1 m, at Le Couye and Jachere, respectively), the suggestion is that the incoming heat fluxes from the atmosphere (above screen-level) were smaller at Le Couye, resulting in lower near-surface temperatures than at Jachere.

The vertical velocity variance (σ_w^2) (Figure 3d), which we use as a measure of vertically oriented turbulence, began to drop rapidly from around 1600 UTC at both sites, but, as with the near-surface temperatures, this drop was more rapid at Le Couye and reached lower values here than at Jachere. The (σ_w^2) thresholds approximated for fog formation (Price, 2019; $0.002\text{--}0.005\text{ m}^2 \cdot \text{s}^{-2}$), below which radiation fog is able to form, are therefore reached earlier in the late afternoon/evening at Le Couye than at Jachere. As well as dropping more quickly, σ_w^2 values at Le Couye also reached lower minima. These lower levels appeared to be maintained for longer at Le Couye. The values observed here remained comfortably under the fog-formation threshold for many hours, whereas at Jachere they were more likely to be borderline. Given that σ_w^2 dropped more rapidly in the late afternoon at Le Couye and remained lower here than at Jachere for multiple hours, it is likely that this was limiting the transfer of heat downwards and therefore allowing more significant cooling at Le Couye, and for fog to form earlier at this site.

The sensible heat-flux data also support this notion (Figure 3e); at Le Couye they remained closer to zero from the time that the sites started to cool compared with Jachere until around the time that the initial fog had formed at Le Couye. Therefore, more heat was moving from the atmosphere towards the near-surface at Jachere compared with Le Couye, reducing the cooling at Jachere compared with Le Couye. These lower values of sensible heat flux towards the surface at Le Couye are most likely a consequence of the very low vertical velocity variance, and we therefore suggest that this reduction in turbulence, which is consistent with sheltering due to the presence of trees around Le Couye, limited the mixing of air near the surface with warmer air aloft, allowing the near-surface to continue to cool rapidly and enabling the earlier formation of fog.

Values of σ_w^2 were assessed at two other heights for each site (23 and 48 m at Le Couye, and 25 and 50 m at Jachere; Figure 4b) and results indicate that the vertical gradient in σ_w^2 was larger at Le Couye, particularly below 25 m altitude from late afternoon onward. This large reduction in σ_w^2 at 2 m relative to the values at 23 and 48 m is consistent with sheltering of the lower levels by

the surrounding trees, which stand at around 10–20 m in height, at Le Couye.

3.5 | Wind speeds

Analysis of wind-speed data at the two sites shows a consistent picture with the turbulence and heat-flux data. Results show that, at around the time at which the temperatures and turbulence intensity lowered, the wind speeds at various heights also reduced. These reductions were observed at both sites, but occurred more rapidly at Le Couye than at Jachere from around 1600 UTC. The wind speeds from 2 m up to 50 m are shown in Figure 5 and have been averaged over 10-min periods. Due to a fault with the anemometer mounted at 10 m at Jachere, these data have only been used when the wind speed was greater than $1.5\text{ m} \cdot \text{s}^{-1}$.

The wind speeds at the three lowest measurement heights all dropped off more rapidly at Le Couye in the late afternoon; this occurred at approximately 1600 UTC during both cases. These then tended to remain lower than those measured at Jachere for at least a few hours; on October 29, the wind speeds between the two sites became much more comparable from approximately 2000 UTC, however during October 28 there were discrepancies between the sets of wind speeds until around 0800 UTC the following morning. Without a daytime heat flux from the surface (transferring momentum down), the increased drag around the trees could reduce winds at Le Couye more rapidly than at Jachere. The wind speeds at the higher measurement heights (48 and 50 m) showed more similarity between the sites, as did the temperatures at this height, although there were still occasions when the wind speeds at Le Couye dropped below those at Jachere; however, these tended to be shorter-lived than at the other heights. This is somewhat in contrast to the temperatures, which exhibited significant differences only below 10 m between the two sites.

The rapid decline in the wind speeds, during both cases, at Le Couye compared with the much more gradual and less consistently decreasing wind speeds at Jachere are consistent with the above argument that Le Couye experienced sheltering from the surrounding trees up to a height of around 10–20 m. This is consistent with Mazoyer *et al.* (2017), who simulated higher wind speeds near the forest area when a tree barrier was removed.

3.6 | Additional cases at the near-surface

Additional cases where radiation fog was observed at Le Couye have been compared with the measurements made

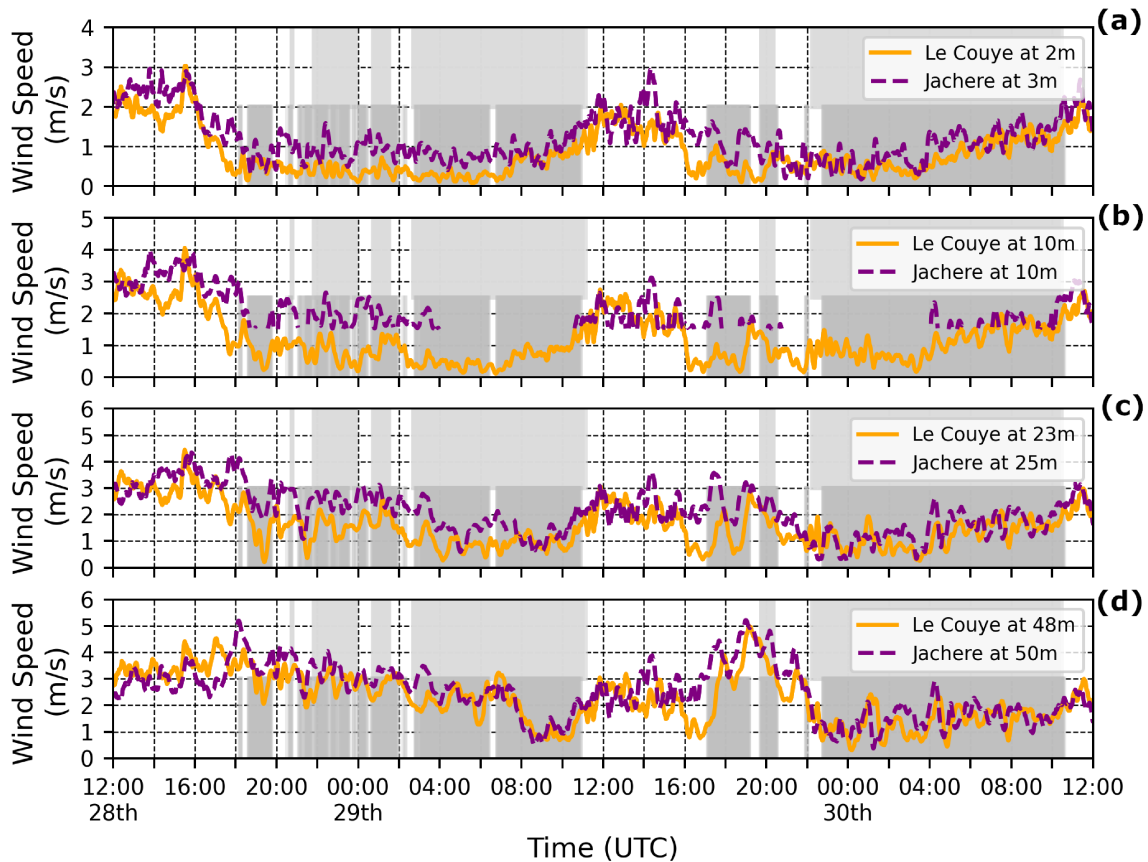


FIGURE 5 The wind speed as measured by sonic anemometers mounted at (a) 2 m, (b) 10 m, (c) 23 m, and (d) 48 m at Le Couye (solid orange), and (a) 3 m, (b) 10 m, (c) 25 m, and (d) 50 m at Jachere (dashed purple).

at Jachere in order to assess whether the early fog formation that was present at Le Couye on October 28 and 29 was a regular feature. As previously mentioned, there are no measurements made at a height greater than 10 m from the beginning of November 2019 at Jachere, and therefore near-surface measurements only are used in this section. Given that the earlier fog formation observed at Le Couye was at 2 m, these near-surface measurements should be adequate in assessing whether it is more common to see fog forming earlier at the sheltered site of Le Couye than at the open site of Jachere.

The six additional dates were selected due to the presence of radiation fog at Le Couye; these cases, along with the two previously mentioned, were chosen due to both (a) the radiation fog being the most persistent it had been over the campaign period (at Le Couye), and (b) data being available for both sites. At Le Couye, each of the radiation fog cases was initially shallow, inhomogeneous, and stable. The fog did not develop into anything deeper for four of the six additional cases presented here. The exceptions included October 31, 2019, where stratus fog was seen in the IR camera footage to advect to the site at around 0100 UTC; this was measured by the visimeters at 23 and 48 m, but not at 2 m. This stratus fog is expected to

be the cause of the drop in visibility at 3 m at Jachere that is illustrated in Figure 6a at around 0100 UTC (the grey shading in the top half of the plot shows where the visibility at Jachere was below 1 km). The other exception was on December 5, 2019, where the shallow, inhomogeneous radiation fog did develop into deep adiabatic fog. This fog was measured by the visimeter at 23 m by around 2200 UTC at Le Couye. Here we focus on the initial fog formation, which remained shallow and inhomogeneous, and do not comment on the later development.

It can be seen in each of the plots in Figure 6 that radiation fog formation occurred earlier at Le Couye than at Jachere (grey shading in lower and upper halves of plot, respectively). This is in line with what was observed during the previous two October case studies. Similarly to these two case studies, early fog formation during the additional six dates also remained shallow and inhomogeneous and dissipated after around two hours, before reforming over an hour later. The air temperature over the additional six cases tended to drop off more rapidly at Le Couye than at Jachere in the late afternoon (Figure 6), and lower temperatures were maintained here for multiple hours. At the time fog formed at Le Couye, the temperature here had dropped below that at Jachere. This also tended to

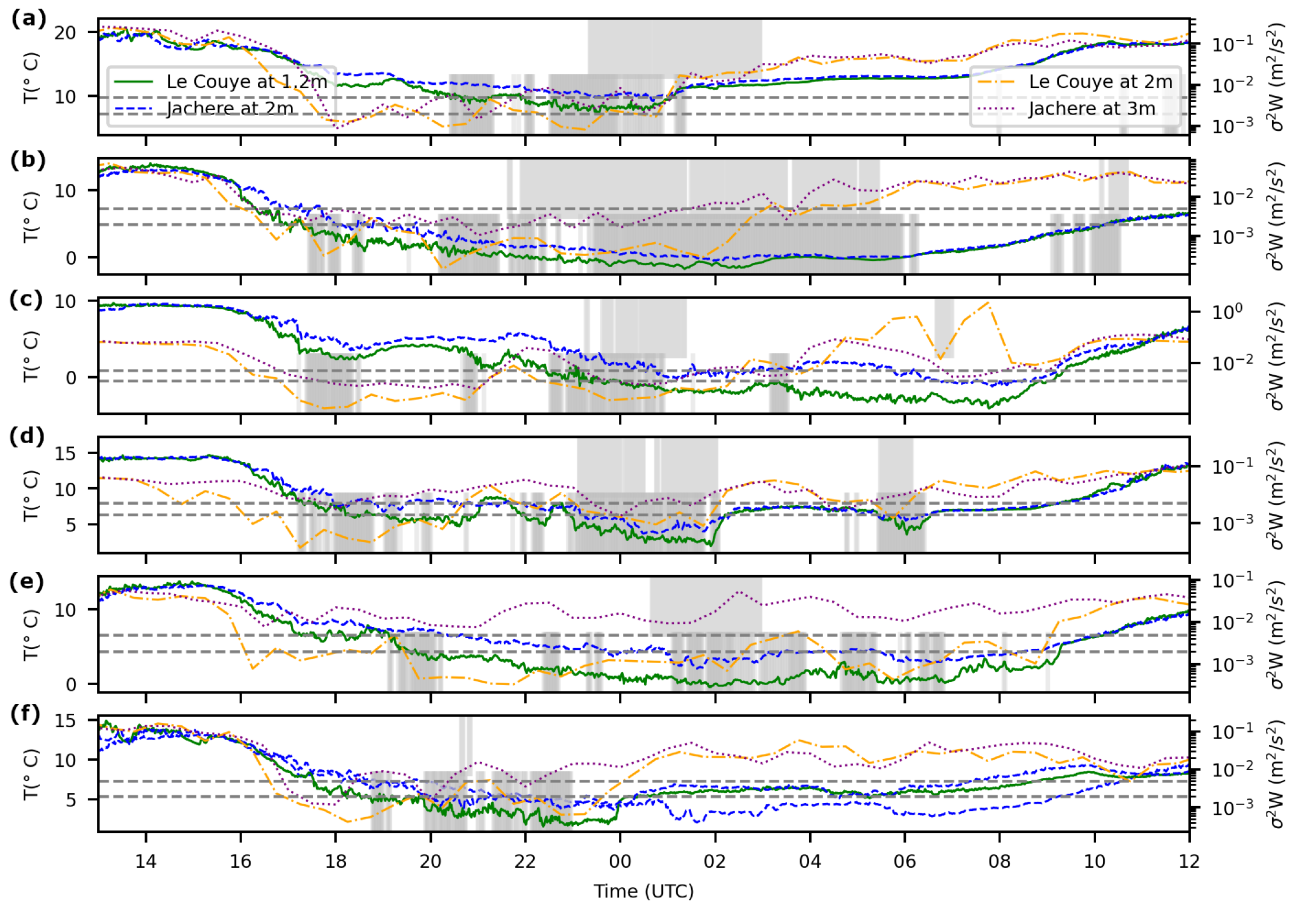


FIGURE 6 The near-surface temperature and vertical velocity variance at Le Couye (green, orange, respectively) and Jachere (blue, purple, respectively) over six different dates where radiation fog was observed at Le Couye: (a) 31/10/19, (b) 05/12/19, (c) 04/01/20, (d) 08/01/20, (e) 24/01/20, (f) 26/01/20. The grey shading in the top and bottom halves of each plot represents the times at which fog was present at the level of the lowest visiometer at Jachere and Le Couye, respectively. The dashed horizontal lines represent the threshold for fog formation as described by Price (2019).

be the case with σ_W^2 (Figure 6). It is certainly clear from Figure 6b–f that σ_W^2 dropped more rapidly in the late afternoon and reached a value lower than that observed at Jachere before the fog formed. An exception to this may be during the October 31, 2019 case (Figure 6a), where σ_W^2 dropped to around the same value by 1800 UTC at the two sites. On this evening, however, early fog formation did not occur until around 2000 UTC, which was the latest occurrence of this across all eight cases reviewed here. Around two hours before the fog formed on October 31, σ_W^2 at Le Couye did drop off, in contrast to that at Jachere, which actually increased. Therefore this case, as with the other seven cases, does support the idea that a greater reduction in σ_W^2 and air temperature near to the surface at Le Couye was enabling the early formation of radiation fog that was not observed at Jachere. The near-surface wind speeds (not shown here) at Le Couye were generally lower than those at Jachere, similarly to previous analysis, again supporting the notion of a sheltering effect caused by the surrounding forested area at Le Couye.

The vertical velocity variance has been plotted against the change in near-surface temperature from the time that the former began to drop (approximately 1600 UTC) at both sites until just before fog formed at Le Couye, over the eight radiation fog cases, in Figure 7a. The plot illustrates that higher rates of cooling occurred at Le Couye in the presence of low turbulence. As σ_W^2 increases, the rate of cooling generally decreases at Le Couye, whereas at Jachere the cooling rate is similar at different values of σ_W^2 . This suggests a greater correlation between the temperature and σ_W^2 at Le Couye. The ratios of dT/dt to σ_W^2 were much higher at Le Couye than at Jachere, 1162 and 378°C hour⁻¹ (m²s⁻²)⁻¹, respectively, illustrating further the higher cooling rates in the presence of lower σ_W^2 at Le Couye. Additionally, Figure 7b presents the difference in specific humidity at the two sites, where a negative value corresponds to a lower specific humidity at Le Couye. These are plotted from approximately 1530 UTC until the time that fog formed at Le Couye for each of the eight radiation fog cases; the cases were treated separately and

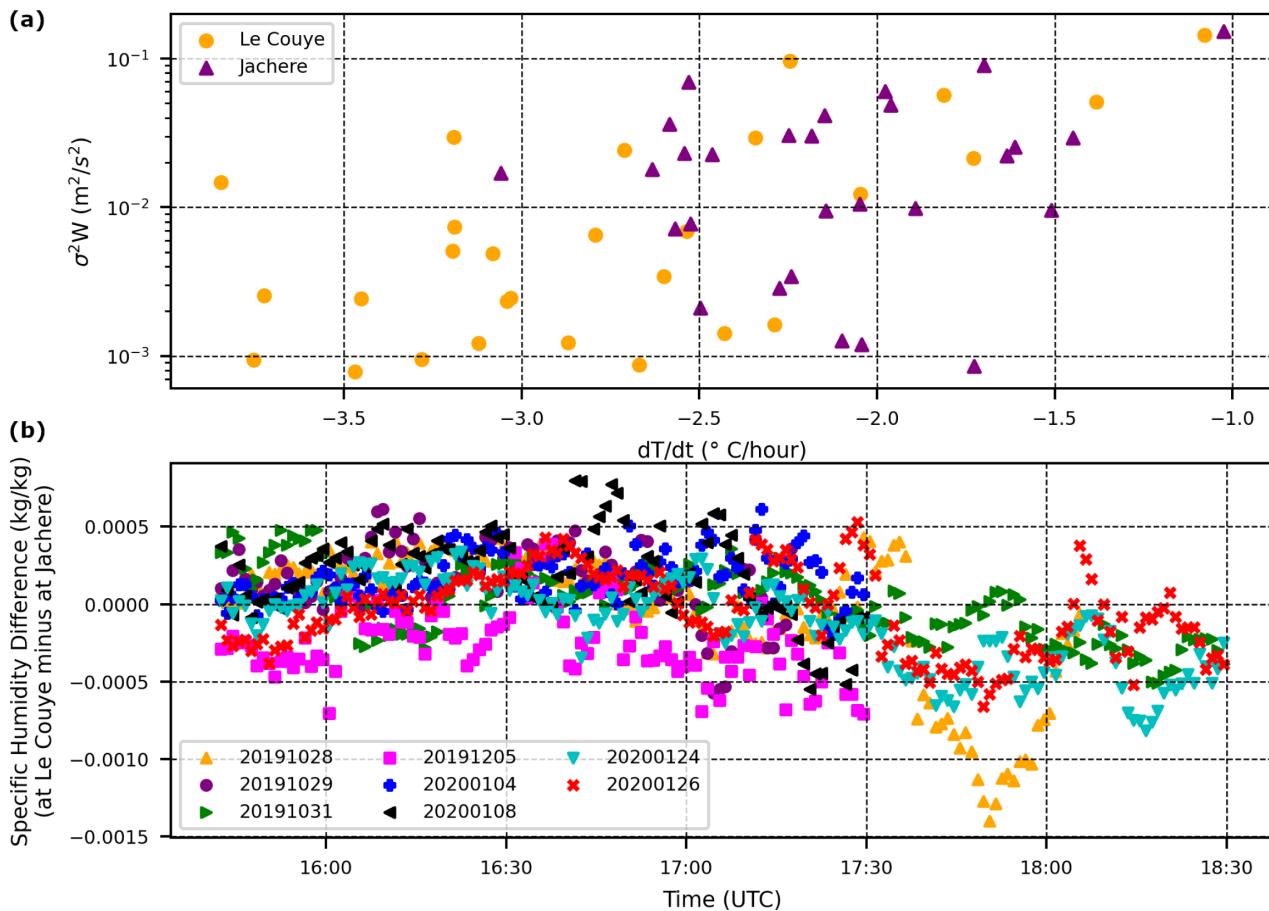


FIGURE 7 (a) σ_w^2 against dT/dt during the period at which the turbulence began to decrease until fog formed at Le Couye, over all eight radiation fog cases, at Le Couye (orange circles) and Jachere (purple triangles); (b) the difference between the specific humidity at Le Couye and Jachere from approximately 1530 UTC until fog formation at Le Couye over each of the eight radiation cases (a negative value corresponds to a lower specific humidity at Le Couye).

therefore the time series ends earlier for some cases where fog formed earlier. The plot suggests a slightly higher near-surface specific humidity at Le Couye in the late afternoon, transitioning to lower values than at Jachere after 1730 UTC. This may be a consequence of dewfall differences at the two sites, with the colder temperatures at Le Couye producing more dew formation. This is, however, outside of the scope of this work, and we present the differences in specific humidity to illustrate that early fog formation at Le Couye occurs under conditions of both lower and higher specific humidity relative to Jachere, suggesting that early fog formation is not a consequence of a higher specific humidity at Le Couye. The two sites have similar surfaces (arable field) and similar soil types, to the best of our knowledge, so it is not expected that the difference in fog formation time is a consequence of surface properties either. Additionally the sites were located on flat ground, with no obvious connection to any cold pool generated by a valley. We therefore conclude, using Figure 5, that the temperature evolution is dominated by

the turbulence, which in turn causes earlier fog formation at Le Couye.

The difference in σ_w^2 between the two sites during the period when fog formed at Le Couye but not at Jachere is shown in Figure 8. The average difference over all eight radiation cases was $0.006 \text{ m}^2 \cdot \text{s}^{-2}$, with the lowest average of $0.001 \text{ m}^2 \cdot \text{s}^{-2}$ occurring for the October 29 case. These small differences highlight how sensitive fog formation is to turbulence levels, and therefore the large challenge to numerical models in forming fog accurately.

4 | COMPARISON WITH ADDITIONAL SITES

Data from additional sites have been introduced to identify any other cases where early fog formation was observed or not. The additional sites were chosen specifically to represent the range between an open site and a very sheltered site. These sites were used to supplement the main sites

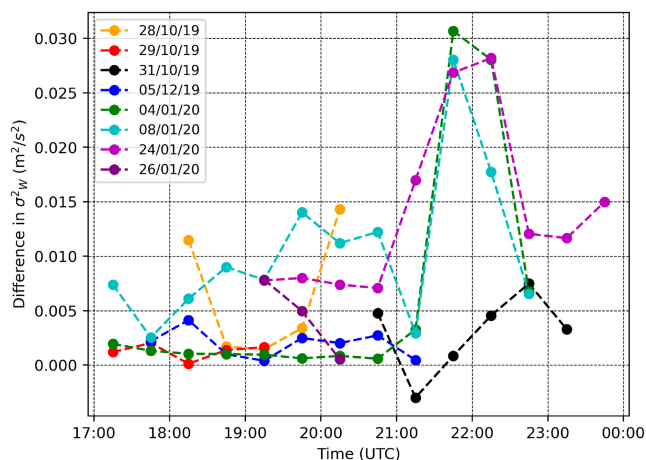


FIGURE 8 The difference in σ_W^2 between Jachere and Le Couye during the period where earlier fog formed at Le Couye until just before fog formed at Jachere, over eight radiation fog cases. The σ_W^2 at 2 m at Le Couye has been subtracted from the σ_W^2 at 3 m at Jachere.

and consequently did not have such an extensive suite of instrumentation. Therefore we are unable to repeat all of the measurement comparisons that have been presented so far, but were able to compare the visibility, temperature, and longwave radiation at the near-surface. As well as Le Couye and Jachere, these sites were the following.

- (1) Basta FMS (fog monitor station) UKMO station was an open site, comparable with Jachere.
- (2) Charbonniere Meteo-France site was a fairly open site, slightly less so than Jachere or Basta.
- (3) Champs-Tanon FMS (fog monitor station) UKMO station was very similar to Le Couye in that it was situated in a maize field with surrounding forested area. The field was approximately $450 \times 950 \text{ m}^2$ at its maximum dimensions.
- (4) Les Houzins Meteo-France station was situated in a large forest clearing and was more sheltered than Le Couye. The clearing had a diameter of approximately 200 m. This site was at the slightly lower altitude of 45 m compared with 70 m at other sites.
- (5) Foret-Tanon was in a narrow forest clearing, which was very sheltered, more so than Les Houzins or Le Couye. The clearing width was approximately 2–3 m, and the trees were around 8–10 m in height.

The instrumentation at each of the more sheltered sites (Le Couye, Champs-Tanon FMS, Les Houzins, and Foret-Tanon) was located approximately in the centre of the clearing.

The near-surface temperatures at these additional sites support the findings so far, that the more sheltered sites

experience lower nocturnal temperatures near to the surface (Figure 9). The more open sites of Jachere, Basta, and Charbonniere show similarity between the measurements and are all generally higher than the temperatures measured at the more sheltered sites of Le Couye, Champs-Tanon, Les Houzins, and Foret-Tanon, which also show similarity between temperature measurements. As well as at Le Couye, shallow fog was also seen to form early at Les Houzins (large forest clearing) compared with the open sites of Jachere and Charbonniere (Figure 10). This could be a consequence of Les Houzins being located at a lower elevation (which would normally be colder during stable boundary-layer conditions) than Jachere and Charbonniere; however, Le Couye is also located at a higher elevation. We suggest therefore that the earlier fog formation at Les Houzins could be a consequence of sheltering by the surrounding forest, as was observed at Le Couye. At Foret-Tanon (narrow forest clearing), early fog formation near to the surface was not observed; instead, the formation of fog tended to occur after it had done so at Jachere. This is despite the near-surface temperatures at Foret-Tanon being similar to those observed at the other three sheltered sites (Le Couye, Les Houzins, Champs-Tanon). It is suggested by the longwave radiation data (not shown here), however, that the near-surface at Foret-Tanon was not cooling radiatively as rapidly in the afternoon as the other two sites (Le Couye and Les Houzins). This is due to higher levels of downwelling longwave radiation, measured near the surface, which could likely be a consequence of the trees emitting additional longwave radiation downwards.

Given that the near-surface of Foret-Tanon was not cooling radiatively, it is possible that the cold air was advecting in from one of the surrounding areas. The Champs-Tanon station was sited in the neighbouring field roughly 200 m south of Foret-Tanon. Although the near-surface temperatures at Champs-Tanon were cooler than those observed at the open site of Jachere (Figure 9), they were very similar to those measured at Foret-Tanon. Given that the surrounding trees were at a distance comparable with those at Le Couye, it is expected that this site had similar amounts of downwelling longwave radiation and the surrounding trees did not influence this to the extent that they had at Foret-Tanon. Champs-Tanon provides evidence that neighbouring areas to Foret-Tanon were cooling rapidly compared with the more open sites. It is possible that this colder air may have advected to Foret-Tanon.

Given that temperatures at Foret-Tanon were similar to those at the sheltered sites, it seems surprising that it experienced less fog at the lowest levels. Indeed, when the visibility dropped below or close to 1 km, it was more likely to do so at 10 m, a similar height to the trees (Figure 10).

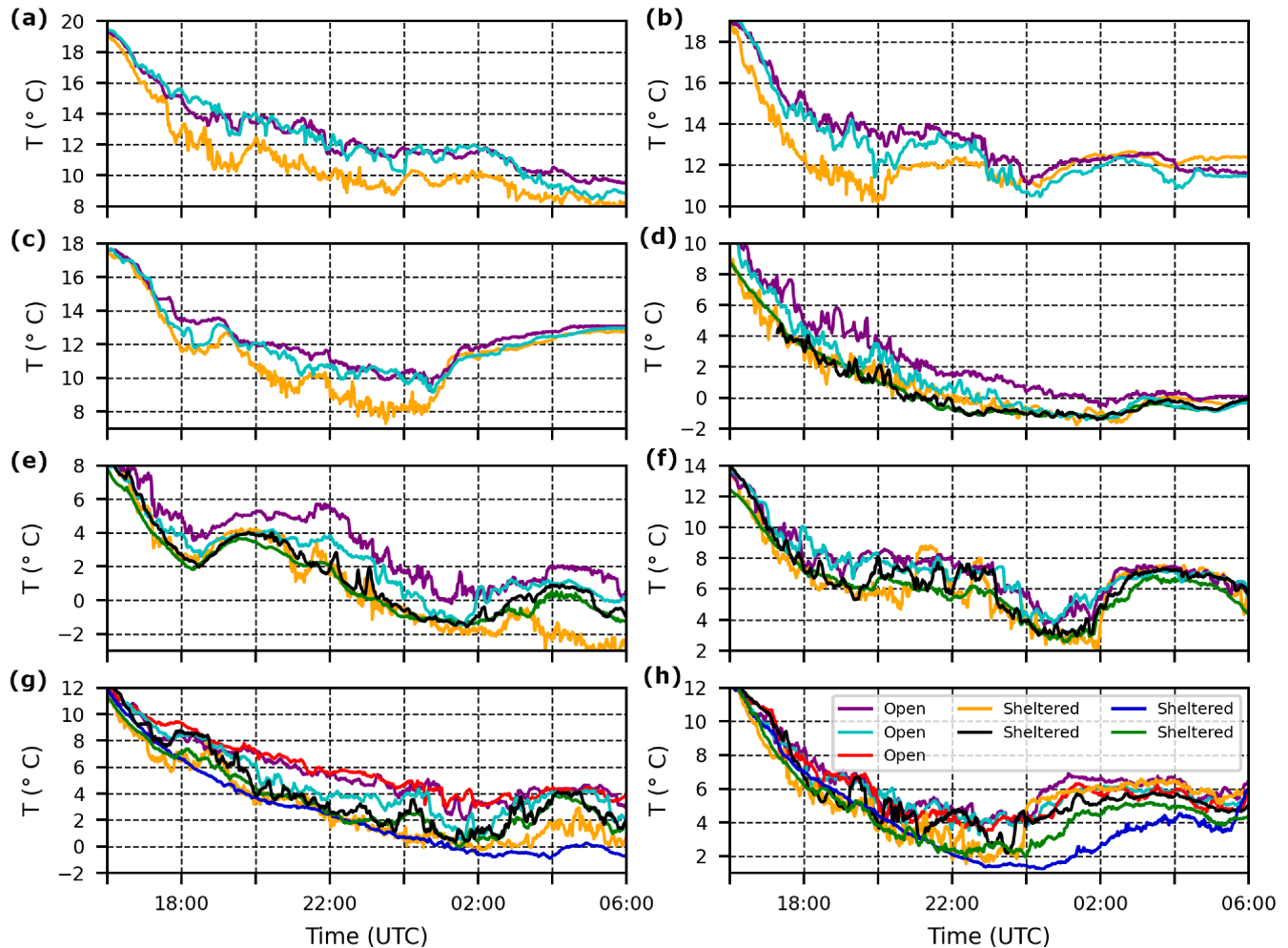


FIGURE 9 The air temperature at 1.2 m at Le Couye (orange), Champs-Tanon (black), and Basta (cyan), and 2m at Jachere (purple), Charbonniere (red), Les Houzins (blue), and Foret-Tanon (green), over eight cases of radiation fog occurrence: (a) 28/10/19, (b) 29/10/19, (c) 31/10/19, (d) 05/12/19, (e) 04/01/20, (f) 08/01/20, (g) 24/01/20, (h) 26/01/20.

Fog may typically have advected at higher levels or formed at tree-top level, similarly to the elevated radiation fog events observed during 88% of fog cases in close proximity to the tree barrier at SIRTa during ParisFOG (Stolaki *et al.*, 2015; Mazoyer *et al.*, 2017). In this case the fog may not always reach the lower canopy due to unfavourable conditions there, that is, greater turbulence, or the fog droplets are deposited onto the vegetation, increasing the visibility. This deposition may also have occurred if the fog instead advected or formed at lower levels. In observations of shallow radiation fog, Price and Stokkerit (2020) shows through IR camera footage that fog can exhibit “sloshing” movements from side to side. The camera footage from Le Couye as part of SOFOG3D (not shown) also reveals this type of behaviour. The consequence of this type of movement across the area surrounding Foret-Tanon would be for the fog to become deposited onto the vegetation at 2 m (within the canopy), but not at 10 m (above the canopy). In

addition, dew may deposit directly onto the trees, reducing the available water for fog. To determine whether water could be deposited onto trees via dew, the 10-m tree temperatures and dewpoint at Le Couye were compared. The tree temperatures were determined from the IR camera footage; grid-box means were estimated, as shown in Figure 11, over two independent areas (boxes 1 and 2; temperature 1 was calculated over the former area and temperature 2 over the latter.). This was executed at periods during the late afternoon and into the evening of two radiation fog events, before the fog had developed vertically to the 23-m visiometer. It is shown in Figure 12 that during both of these cases the tree temperatures became comparable to the dewpoint temperature before the fog had developed vertically. Therefore it is possible for water vapour to have been condensed onto the trees here, causing fog formation to be inhibited in the forested area. If we assume that the tree temperature at Foret-Tanon behaved similarly, relative

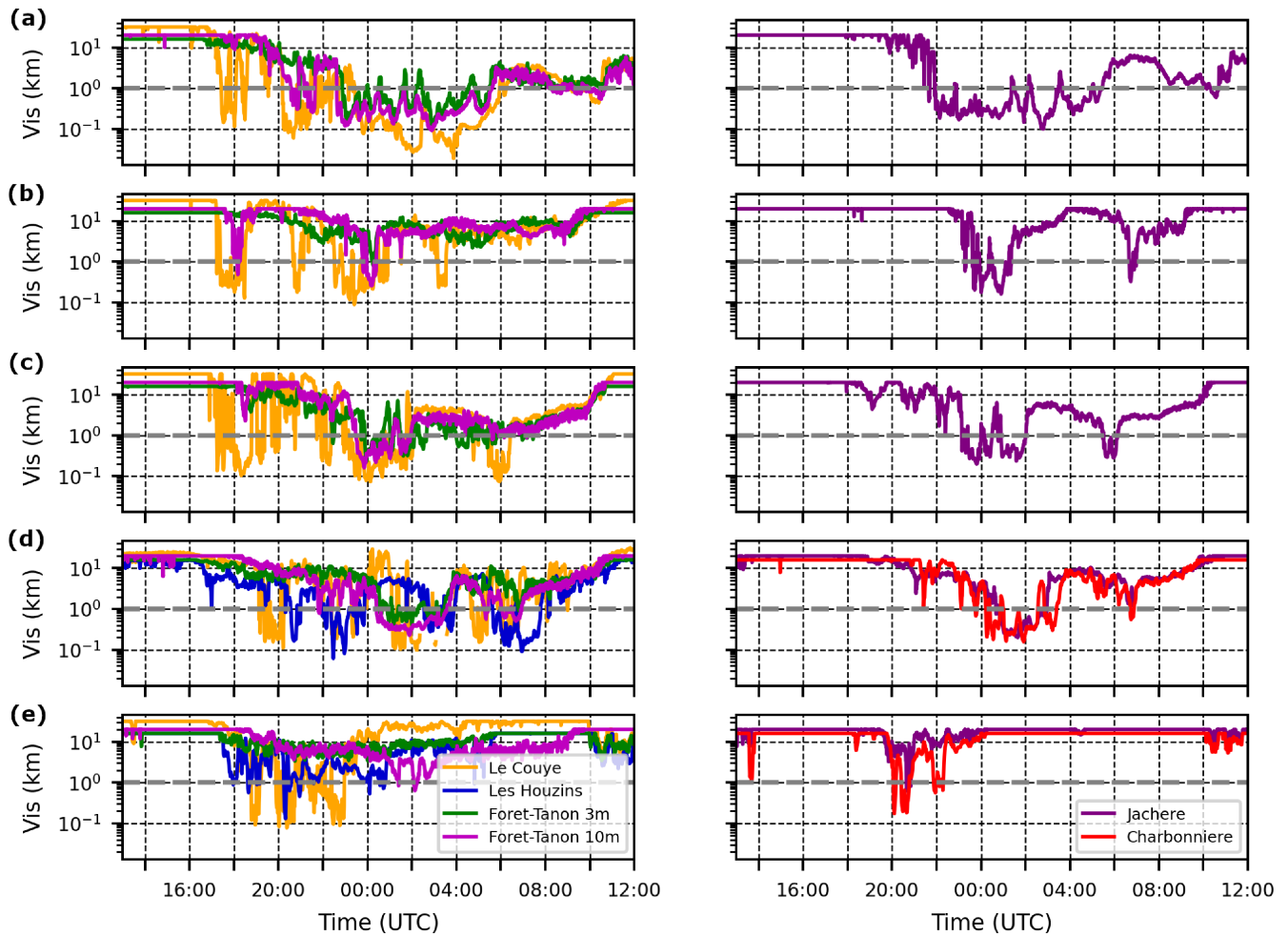


FIGURE 10 The visibility at 2 m at Le Couye (orange), 3 m at Jachere (purple), Charbonniere (red), Les Houzins (blue), and Foret-Tanon (green), and 10 m at Foret-Tanon (magenta) over five cases of radiation fog occurrence: (a) 05/12/19, (b) 04/01/20, (c) 08/01/20, (d) 24/01/20, (e) 26/01/20. The first column contains visibility measured at sheltered sites only, and the second column shows visibility measured at the more open sites.

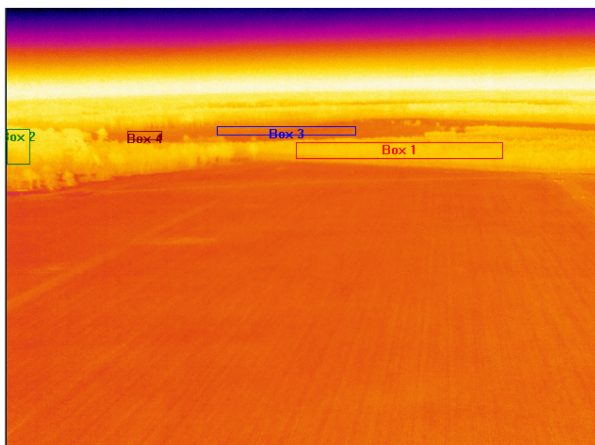


FIGURE 11 Image from an infrared camera mounted at 48 m at Le Couye; mean temperatures were calculated over each of the different boxes. The temperatures from boxes 1 to 2 were used as two separate measurements of tree temperature at approximately 10 m.

to the dewpoint temperature, to that at Le Couye, then it is plausible that, despite the low near-surface temperatures, the visibility did not drop below 1 km due to water vapour condensing onto the vegetation. We appreciate that this theory is speculative, but include it to introduce the idea, which could be explored further in future work, rather than to provide a definitive answer as to why shallow fog formation at Foret-Tanon did not occur as readily as in the larger forest clearings. There were not enough observations at Foret-Tanon to provide conclusive evidence as to why this occurred.

Whatever the mechanism responsible for inhibiting low-level fog formation at Foret-Tanon, it appears from these comparisons that there is significant variability between the sites, influenced by surface heterogeneities. There appears to be a scale of openness somewhere between very open sites (Jachere, Charbonniere) and very narrow forest clearings (Foret-Tanon), where fog

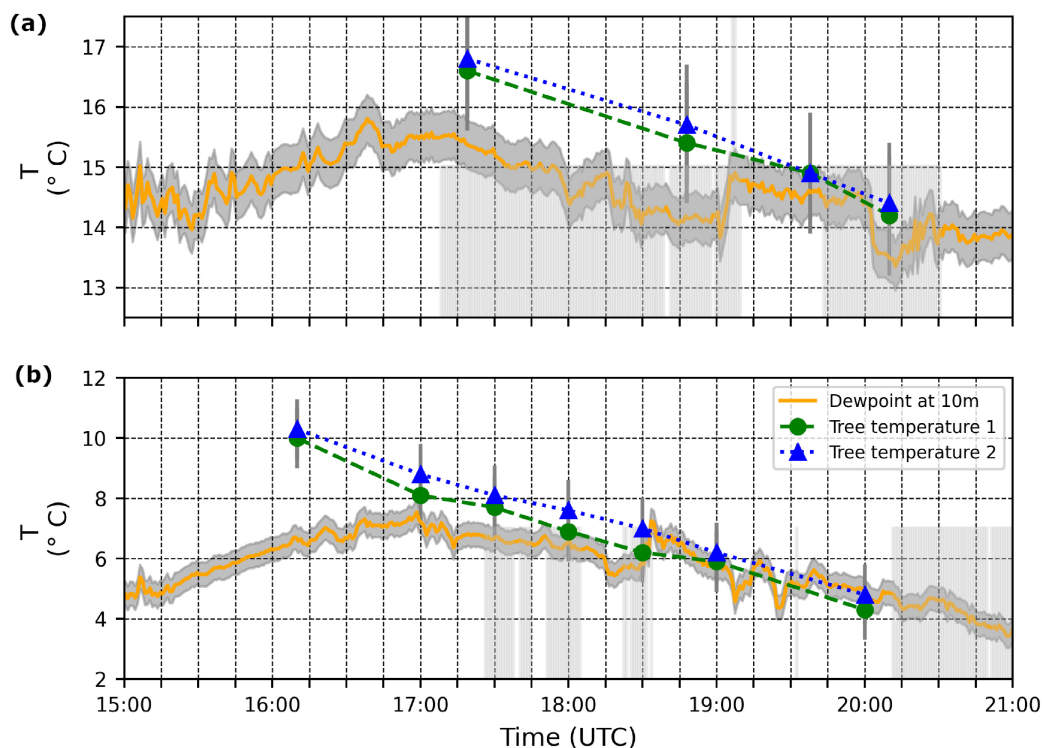


FIGURE 12 The dewpoint temperature (solid orange line) and the mean tree temperatures (green circles, blue triangles) at 10 m at Le Couye, over two cases of radiation fog occurrence: (a) 29/10/19, (b) 05/12/19. Tree temperature 1 (green circle, dashed line) and tree temperature 2 (blue triangle, dotted line) were calculated over the areas described by boxes 1 and 2, respectively, in Figure 11. The horizontal light grey shading represents cases when fog was measured at 2 m at Le Couye. The darker grey shading surrounding the dewpoint temperature line represents the error in the measurement.

formation is enhanced by sheltering from the surrounding forested area (Le Couye, Les Houzins).

5 | SUMMARY AND CONCLUSIONS

As part of the SOFOG3D project, we have analysed data from two 50-m mast sites over two cases of radiation fog formation and development. The two sites differed in their surroundings: Jachere was very open on agricultural land, and Le Couye was located within an agricultural field, which was surrounded by forested area. We supplemented these cases with six other radiation fog cases, and data from five additional sites, for which we had near-surface measurements available.

We found that, in all eight cases of radiation fog, formation occurred earlier at Le Couye than at Jachere. These were cases of in situ formation, where the fog remained shallow and dissipated after around 2 hr. For the two radiation fog cases that occurred whilst the 50-m masts were erected, we attribute this dissipation to cloud passing over the site. When the cloud had passed for the final time, we observed the fog reforming at Le Couye and also forming at Jachere around the same time. This fog was able to develop

vertically at both sites, and the fog lifted at the same time on the following morning, likely as a result of solar insolation. We found that the near-surface air temperature at Le Couye tended to drop more rapidly and reached lower values from around 1600 UTC for all of the radiation fog cases. For the two 50-m mast cases, we found that as the measurement height increased the temperatures at the two sites became more comparable; at roughly 25 and 50 m the temperatures were approximately the same. Additionally, we find that there is no significant difference in specific humidity between the two sites.

We suggest that the reason for the lower near-surface temperatures at Le Couye was a consequence of the surrounding trees providing a sheltering effect and reducing the amount of turbulence at the lowest levels. This is reflected in the vertical velocity variance (σ_w^2) measurements, which, similarly to the temperatures, drop off more rapidly at Le Couye in the late afternoon. This limits the mixing of the near-surface air with the warmer air aloft, and therefore allows the near-surface to cool rapidly via radiation and fog to form. This is in agreement with Price (2019), who found that the foggiest of the LAN-FEX sites were those where (σ_w^2) was more consistently below $0.005 \text{ m}^2 \cdot \text{s}^{-2}$. The difference in σ_w^2 between the

two sites during the period when fog formed at Le Couye but not at Jachere was shown to be very small, subsequently highlighting how sensitive the fog formation is to the turbulence levels, and therefore the large challenge to numerical models in forming fog accurately. Additionally, we observed that the nocturnal σ_w^2 , from the late afternoon, at the near-surface tended to be consistently lower than at the other two heights (23 and 48 m) at Le Couye, whereas at Jachere it was similar throughout at all three measurement heights. The increased sheltering therefore creates stronger gradients between approximately 10 and 25 m in both temperature and turbulence (noting that the tree heights were in the region of 10–20 m). These results were consistent for all of the cases examined. In agreement with the sheltering effect, we found that the wind speeds at Le Couye were lower from the late afternoon than at Jachere.

We were unable to compare σ_w^2 measurements at the additional sites, since these were more minimally instrumented, but we found that those that were surrounded by forested area exhibited similar near-surface temperature to each other, and tended to be lower than the equivalent measurements at the more open sites. Similarly, the near-surface temperatures at the open sites were all similar to each other. Although the temperatures at the more sheltered sites were comparable, those measured at the most narrow forest clearing did not appear to be driven by radiative cooling to the same extent as the other sites in the late afternoon. This is a possible reason as to why early fog formation was not observed at the near-surface at this site. Another is that water was deposited onto the vegetation. Fog, however, was observed earlier at the other two sheltered sites than at the more open sites. These two sites, Le Couye and Les Houzins, were in much larger clearings than the site in the narrow clearing (Foret-Tanon). It is therefore possible that there is a limit, at both ends of the scale, to the amount of sheltering provided by trees, which enables fog to form more readily. We have shown here that this fog formation could be enabled by rapid drop-offs in vertical velocity variance due to a sheltering effect, which limits the amount of turbulent mixing and allows the near-surface to cool more rapidly during the evening.

The results have shown that these differences are mostly confined to the earlier stages of fog development and last for periods up to a few hours. If the atmosphere becomes generally saturated at higher levels, the differences in fog morphology at the various locations disappear and the fog field appears more homogeneous on larger scales. A remaining question is the extent to which earlier shallow fog formation in clearings influences subsequent deeper and more widespread formation. For example, could a few clearings in a more generally open landscape cool the air sufficiently to reduce temperatures over a

wider region and hence allow fog to form that otherwise would not? More specifically, would a widespread regional fog develop later, if the shallower fog in clearings did not form initially? Notwithstanding this, the results found in this study indicate that accurate forecasting of shallow fog on small scales requires a very detailed knowledge of local topography, which is likely to prove challenging for numerical models to forecast accurately. This work highlights a need for further measurement campaigns to explore the fog life cycle on a very fine scale within forests and their surroundings to describe the transition from forest to clearing better. The inclusion of model simulations to explore the transition could support and possibly quantify further the findings from this work. This could use LES model simulations at approximately the same resolution as in Mazoyer *et al.* (2017) (~5m) to characterise the immediate vicinity of the forest better, helping to distinguish its effect on the formation of fog within clearings.

AUTHOR CONTRIBUTIONS

J. Thornton: formal analysis; writing – original draft. **J. D. Price:** writing – original draft; writing – review and editing. **F. Burnet:** conceptualization. **C. Lac:** conceptualization; writing – review and editing.

ORCID

J. Thornton  <https://orcid.org/0000-0002-8350-4823>

F. Burnet  <https://orcid.org/0000-0003-0572-4422>

C. Lac  <https://orcid.org/0000-0003-0324-3991>

REFERENCES

- Ahmed, M.M., Abdel-Aty, M., Lee, J. and Yu, R. (2014) Real-time assessment of fog-related crashes using airport weather data: a feasibility analysis. *Accident Analysis & Prevention*, 72, 309–317.
- Bergot, T. (2013) Small-scale structure of radiation fog: a large-eddy simulation study. *Quarterly Journal of the Royal Meteorological Society*, 139(673), 1099–1112.
- Boutle, I., Angevine, W., Bao, J.-W., Bergot, T., Bhattacharya, R., Bott, A., Ducongé, L., Forbes, R., Goecke, T. and Grell, E. (2022) Demistify: a large-eddy simulation (les) and single-column model (scm) intercomparison of radiation fog. *Atmospheric Chemistry and Physics*, 22(1), 319–333.
- Burnet, F., Lac, C., Martinet, P., Fourrié, N., Haeffelin, M., Delanoë, J., Price, J., Barrau, S., Canut, G., Cayez, G., Dabas, A., Denjean, C., Dupont, J., Honnert, R., Mahfouf, J., Montmerle, T., Roberts, G., Seity, Y. and Vié, B. (2020) The South west FOGs 3D experiment for processes study (SOFOG3D) project. *EGU General Assembly Conference Abstracts*, page 17836.
- Chachere, C.N. and Pu, Z. (2019) Numerical simulations of an inversion fog event in the salt lake valley during the materhorn-fog field campaign. *Pure and Applied Geophysics*, 176(5), 2139–2164.
- Cuxart, J. and Jiménez, M. (2012) Deep radiation fog in a wide closed valley: study by numerical modeling and remote sensing. *Pure and Applied Geophysics*, 169(5), 911–926.

- Gultepe, I., Fernando, H., Pardyjak, E., Hoch, S., Silver, Z., Creegan, E., Leo, L., Pu, Z., De Wekker, S. and Hang, C. (2016) An overview of the materhorn fog project: observations and predictability. *Pure and Applied Geophysics*, 173(9), 2983–3010.
- Gultepe, I., Pearson, G., Milbrandt, J., Hansen, B., Platnick, S., Taylor, P., Gordon, M., Oakley, J. and Cober, S. (2009) The fog remote sensing and modeling field project. *Bulletin of the American Meteorological Society*, 90(3), 341–360.
- Gultepe, I., Sharman, R., Williams, P.D., Zhou, B., Ellrod, G., Minnis, P., Trier, S., Griffin, S., Yum, S. and Gharabaghi, B. (2019) A review of high impact weather for aviation meteorology. *Pure and Applied Geophysics*, 176(5), 1869–1921.
- Gultepe, I., Tardif, R., Michaelides, S.C., Cermak, J., Bott, A., Bendix, J., Müller, M.D., Pagowski, M., Hansen, B. and Ellrod, G. (2007) Fog research: a review of past achievements and future perspectives. *Pure and Applied Geophysics*, 164(6), 1121–1159.
- Haefelin, M., Bergot, T., Elias, T., Tardif, R., Carrer, D., Chazette, P., Colomb, M., Drobinski, P., Dupont, E. and Dupont, J.-C. (2010) Parisfog: shedding new light on fog physical processes. *Bulletin of the American Meteorological Society*, 91(6), 767–783.
- Kapoor, P. (2019) Over 10,000 lives lost in fog-related road crashes. <https://timesofindia.indiatimes.com/india/over-10000-lives-lost-in-fog-related-road-crashes/articleshow/67391588.cms>.
- Köhler, C., Steiner, A., Saint-Drenan, Y., Ernst, D., Bergmann-Dick, A., Zirkelbach, M., Bouallegue, Z.B., Metzinger, I. and Ritter, B. (2017) Critical weather situations for renewable energies—part b: low stratus risk for solar power. *Renewable Energy*, 101, 794–803.
- Kulkarni, R., Jenamani, R.K., Pithani, P., Konwar, M., Nigam, N. and Ghude, S.D. (2019) Loss to aviation economy due to winter fog in New Delhi during the winter of 2011–2016. *Atmosphere*, 10(4), 198.
- Mazoyer, M., Lac, C., Thouron, O., Bergot, T., Masson, V. and Musson-Genon, L. (2017) Large eddy simulation of radiation fog: impact of dynamics on the fog life cycle. *Atmospheric Chemistry and Physics*, 17(21), 13017–13035.
- Pauli, E., Cermak, J. and Teuling, A.J. (2022) Enhanced nighttime fog and low stratus occurrence over the landes forest, France. *Geophysical Research Letters*, 49(5), e2021GL097058.
- Price, J. (2011) Radiation fog. Part i: observations of stability and drop size distributions. *Boundary-Layer Meteorology*, 139(2), 167–191.
- Price, J. and Stokkerei, K. (2020) The use of thermal infra-red imagery to elucidate the dynamics and processes occurring in fog. *Atmosphere*, 11(3), 240.
- Price, J.D. (2019) On the formation and development of radiation fog: an observational study. *Boundary Layer Meteorology*, 172, 167–197.
- Pu, Z., Chachere, C.N., Hoch, S.W., Pardyjak, E. and Gultepe, I. (2016) Numerical prediction of cold season fog events over complex terrain: the performance of the wrf model during materhorn-fog and early evaluation. *Pure and Applied Geophysics*, 173(9), 3165–3186.
- Roach, W. (1995) Back to basics: fog: part 2—the formation and dissipation of land fog. *Weather*, 50(1), 7–11.
- Roach, W., Brown, R., Caughey, S., Garland, J. and Readings, C. (1976) The physics of radiation fog: I—a field study. *Quarterly Journal of the Royal Meteorological Society*, 102(432), 313–333.
- Rotach, M.W. and Zardi, D. (2007) On the boundary-layer structure over highly complex terrain: key findings from map. *Quarterly Journal of the Royal Meteorological Society: A Journal of the Atmospheric Sciences, Applied Meteorology and Physical Oceanography*, 133(625), 937–948.
- Scherrer, S.C. and Appenzeller, C. (2014) Fog and low stratus over the swiss plateau—a climatological study. *International Journal of Climatology*, 34(3), 678–686.
- Smith, D., Renfrew, I., Price, J. and Dorling, S. (2018) Numerical modelling of the evolution of the boundary layer during a radiation fog event. *Weather*, 73(10), 310–316.
- Smith, D.K., Renfrew, I.A., Dorling, S.R., Price, J.D. and Boutle, I.A. (2021) Sub-km scale numerical weather prediction model simulations of radiation fog. *Quarterly Journal of the Royal Meteorological Society*, 147(735), 746–763.
- Steenefeld, G., Ronda, R. and Holtslag, A. (2015) The challenge of forecasting the onset and development of radiation fog using mesoscale atmospheric models. *Boundary-Layer Meteorology*, 154(2), 265–289.
- Steenefeld, G., Wokke, M., Groot Zwaafink, C., Pijlman, S., Heusinkveld, B., Jacobs, A. and Holtslag, A. (2010) Observations of the radiation divergence in the surface layer and its implication for its parameterization in numerical weather prediction models. *Journal of Geophysical Research: Atmospheres*, 115(D6).
- Stolaki, S., Haefelin, M., Lac, C., Dupont, J.-C., Elias, T. and Masson, V. (2015) Influence of aerosols on the life cycle of a radiation fog event. A numerical and observational study. *Atmospheric Research*, 151, 146–161.
- Tudor, M. (2010) Impact of horizontal diffusion, radiation and cloudiness parameterization schemes on fog forecasting in valleys. *Meteorology and Atmospheric Physics*, 108(1), 57–70.
- Van der Velde, I., Steenefeld, G., Schreur, B.W. and Holtslag, A. (2010) Modeling and forecasting the onset and duration of severe radiation fog under frost conditions. *Monthly Weather Review*, 138(11), 4237–4253.
- Wærsted, E.G., Haefelin, M., Steenefeld, G.-J. and Dupont, J.-C. (2019) Understanding the dissipation of continental fog by analysing the lwp budget using idealized les and in situ observations. *Quarterly Journal of the Royal Meteorological Society*, 145(719), 784–804.

How to cite this article: Thornton, J., Price, J.D., Burnet, F. & Lac, C. (2023) Contrasting the evolution of radiation fog over a heterogeneous region in southwest France during the SOFOG3D campaign. *Quarterly Journal of the Royal Meteorological Society*, 1–19. Available from: <https://doi.org/10.1002/qj.4558>

APPENDIX

A list of instrumentation located at the UK Met Office and Meteo-France sites, along with their associated uncertainties and sampling and logging frequencies, is provided in Tables A1 and A2, respectively. Only instrumentation used to make the measurements presented within this work is shown.

TABLE A1 Instruments used at the Le Couye site and the Basta and Champs-Tanon fog monitor stations during SOFOG3D.

Measurement (height)	Instrument	Uncertainty	Sampling/ logging frequency
Visibility (2, 23, and 48 m)	Campbell Scientific CS120	10%	1 Hz/1 min
Temperature (1.2, 23 m, and 48 m)	PRTs: PT100 IEC60751 "A"	0.1 °C	1 Hz/1 min
Temperature (skin)	Heitronics KT19 II, KT-15D IRTs	1 °C	1 Hz/1 min
Longwave radiation (m)	Kipp and Zonen, CG4	< 4 W·m ⁻²	1 Hz/1 min
Shortwave radiation (m)	Kipp and Zonen, CMP21, CMP22	< 7 W·m ⁻²	1 Hz/1 min
Soil heat flux (2-cm subsoil)	Hukseflux HFP01SC-10	20%	1 Hz/1 min
Wind speed (2, 10, 23, 48 m)	Gill HS50 sonic anemometer	2%	10 Hz
Vertical velocity (2, 23, 48 m)	Gill HS50	20%	10 Hz
Relative humidity (1.2 m)	Vaisala HMP155	1–2%	1 Hz/1 min
Pressure (2 m)	Delta T, BS5-117	1 hPa	1 Hz/1 min
IR temperature imaging (48 m)	FLIR SC-655 IR camera	1 °C	50 Hz

Note: Only measurements (and instruments) used in this work are listed.

TABLE A2 Instruments used at the Jachere site during SOFOG3D.

Measurement (height)	Instrument	Uncertainty	Sampling/ logging frequency
Visibility (3 m)	Vaisala PWD 22/52	10%	25 s/1 min
Visibility (25 and 48 m)	Young Sentry 73,000	10%	30 s/1 min
Temperature (2, 10, 25, and 45 m)	Thermo Est PT100	0.1 °C	10 s/1 min
Longwave radiation (1 m)	Kipp and Zonen, CNR4	< 4 W·m ⁻²	10 s/1 min
Shortwave radiation (1 m)	Kipp and Zonen, CNR4	< 7 W·m ⁻²	10 s/1 min
Soil heat flux (2-cm subsoil)	Hukseflux HFP01	20%	10 s/1 min
Wind speed (3, 25, and 50 m)	Metek 3 Class AH sonic anemometer	1.5%	50 Hz
Wind speed (10 m)	Young Wind Monitor	0.3 m · s ⁻¹ (above 1.1 m · s ⁻¹)	1 s/1 min
Vertical velocity variance (3, 25, and 50 m)	Metek 3 Class AH sonic anemometer	20%	50 Hz
Relative humidity (2 m)	Vaisala HMP110	5%	10 s/1 min
Pressure (0.3 m)	Vaisala PTB210	0.5 hPa	10 s/1 min

Note: Instruments used at Charbonniere, Champs-Tanon, Les Houzins, and Foret-Tanon were the same as at Jachere for temperature (2 m), humidity(2 m), pressure (0.3 m), and wind (10 m), except for radiative measurements that were performed by a Kipp and Zonen CNR1 probe (1 m), and visibility with a Young Sentry 73000 (3 m) and a PWD 25/52 (10 m) at Foret-Tanon only. Only measurements (and instruments) used in this work are listed.